Molecular Outgassing and Deposition in EP Applications

IEPC-2015-361/ISTS-2015-b-361

Presented at Joint Conference of 30th International Symposium on Space Technology and Science, 34th International Electric Propulsion Conference and 6th Nano-satellite Symposium
Hyogo-Kobe, Japan
July 4–10, 2015

Lubos Brieda*
Particle In Cell Consulting LLC, Falls Church, VA 22046

This paper reports a new model for the gas-surface interface, specifically as applicable to vacuum chamber testing of electric propulsion (EP) devices. The working pressure in vacuum chambers is due to the balance between gas sources and sinks, with sources including, among others, material outgassing and surface desorption. Water vapor desorbing from large-area surfaces dominates the initial environment. Once sources of water are depleted, gases such as nitrogen take the dominant role. Of course, in the case of EP testing, the thruster propellant will be a large contributor to the total pressure. The resulting spatial and temporal variation in species distribution and the total pressure has an important implication to EP testing. Yet, state of the art EP simulation codes do not take into account the details of the vacuum chamber environment. Background pressure is either assumed to be uniform and time invariant, or if the background population is modeled, the codes assume some predefined sticking coefficients. The model presented in this paper instead relies on surface temperature and activation energy to compute residence time, and allows molecules of different materials to deposit on top of a native substrate. The substrate itself may contain trapped gases which gradually diffuses to the surface and eventually desorb. The model is demonstrated by presenting results from three distinct configurations: gas injection into a chamber, outgassing from a test article, and a plasma thruster operating in chamber equipped with a beam dump.

I. Introduction

The familiar "new car smell" is due to unspent hydrocarbons diffusing out of materials making up the car interior. Similar reaction happens when materials are exposed to the vacuum environment. While organic materials outgas hydrocarbons capable of contaminating sensitive components, even non-organics can be a source of volatile gases such as water or nitrogen that contribute to the chamber pressure. For each species, the partial pressure is governed by a balance between sources and sinks. The sinks include mechanical pumps and surfaces cold enough to condense the gas (such us cryopumps and scavenger plates). The sources encompass outgassing and surface desorption, depressurization of air pockets, vacuum chamber leaks, and, in the case of electric propulsion (EP), the injected propellant. Adding up the partial pressures, we end up with the typical operating pressures during EP testing somewhere between 0.5 to 2×10^{-5} Torr.[1] Assuming 300K temperature, ideal gas law $P = nkT$ tells us that the corresponding gas density ranges from 1 to 6×10^{17} m^{-3}. This value is of similar magnitude to the density of un-ionized propellant in the near plume of EP devices.[2] As such, facility background pressure is expected to play an important role in the performance of the device. Such is in fact the case, as has been demonstrated repeatedly by experiments.[3–5] Experimental evidence suggests that changing background pressure not only broadens the beam divergence, but, at least in the case of the Hall thruster, can also alter the discharge behavior.

Yet, despite these observations, state of the art EP plume simulation tools such as Coliseum/Draco[6,7] do not model the chamber background in great detail. The facility effect is commonly introduced only in

*Contact email: lubos.brieda@particleincell.com

the form of uniform background density that does not change with time. This simplification is partly driven by computational resources: the effort expended simulating the background population can be dedicated to resolving the ion beam constituents. But it is also due to limitation of the available models. Draco, just like other similar tools, uses surface sources to inject gases at user-predefined flow rates. The code lacks the capability to automatically model outgassing or surface desorption. It also utilizes user-defined sticking coefficients to determine whether a molecule reflects after impacting a surface. This approach is common industry-wide, and is also used by the radiative heat transfer and molecular contamination communities.

In this paper, we present a novel approach for the surface interface. Instead of utilizing sticking coefficients, the model uses activation energies and surface temperatures to compute molecular residence times. This allows the algorithm to determine whether the molecule "sticks" based on the instantenuous surface temperature. Adsorbed molecules are added to a surface layer. A separate outgssing algorithm pushes gases trapped in the object substrate to the surface. It also computes desorption of materials into the gas phase, again based on the surface temperature and activation energy. Besides being bases on physical parameters, the model also captures the dynamic behavior observed in vacuum chamber testing, including depletion of outgassing materials, and flash-off of condensed matter with a thermal transition. Details of the model are presented in the next section. The model is then demonstrated on several cases covering situations encountered during vacuum and electric propulsion testing, including: gas injection, outgassing, and electric propulsion testing.

II. Surface Model

The model is based on the conceptual view shown in Figure 1. The object placed in the vacuum environment consists of a native substrate, containing arbitrary number of trapped gases. At the surface is a thin layer composed of an arbitrary combination of adsorbed species. The gases trapped in the substrate diffuse towards the surface by process known as outgassing. At the surface, the thin film desorbs, liberating the adsorbed molecules into the bulk gas phase. At the same time, molecules from the external environment impact the surface, and possibly adsorb. There are additional processes taking place, including sputtering, secondary electron emission, and dust particulate deposition. While these processes play an important role, they are beyond the scope of the work presented in this paper.

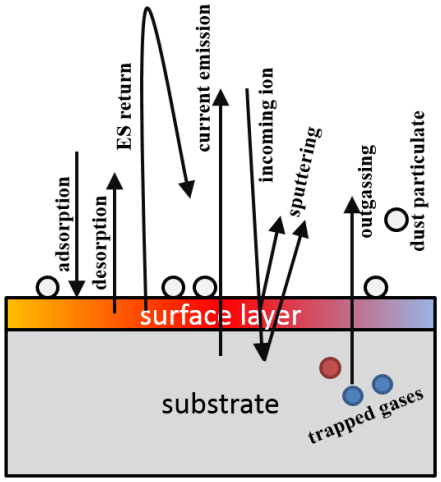

Figure 1. Detailed surface interaction model. Only outgassing and surface adsorption/desorption are considered in this work.

The amount of trapped gases can be specified by their mass. This is the approach taken in our model. Each geometry component (corresponding to a physical object such as thruster body) is initialized with a list of trapped materials and their mass fractions, along with the total mass. At the surface, it is customary to list the molecular contamination cleanliness level. Level A corresponds to surface mass density of $1\mu g/cm^2$, or 100Å, assuming typical contaminant density of $1g/cm^3$. Instead of using cleanliness levels, we specify the thickness of the surface layer directly. The surface layer can be composed of multiple materials.

A. Outgassing

The amount of mass lost to diffusion is given by[8]

$$\frac{dm}{dt} = Cm\frac{\exp(-E_a/RT)}{\sqrt{t}} \tag{1}$$

where the $\sqrt{t}$ term in the dominator is the decay rate for a diffusion-limited process. C is a reaction constant, E_a is the material activation energy (typically in kcal/mol), R is the gas constant (kcal K/mole), and T is the temperature (K). The reaction constant can be determined experimentally using an industry standard test known as ASTM E 595. In this test, a sample is heated and held at 125°C for 24 hours at a pressure less than 5×10^{-5} Torr. The total mass loss (TML) is determined by comparing the final and initial mass of the sample. During the test, a plate held at 25°C is used to measure the amount of material that would condense on a colder (but yet relatively warm) surface. This collected mass is known as collected volatile condensable material (CVCM). Typically, all materials used on spacecraft must exhibit less than 1% TML and 0.1% CVCM.[8] Third parameter, known as water vapor regained (WVR) is measured by subjecting the test sample to 50% relative humidity at 23°C for 24 hours and determining the new mass. This parameter characterizes what percentage of the TML corresponds to water vapor. Detailed listing of parameters for a large list of materials has been compiled by Campbell and Scialdone.[9] Integrating Equation 1 allows us to determine the mass remaining after some time t,

$$m_2 = m_1 \exp\left[-C\exp(-E_a/RT)2t^{1/2}\right] \tag{2}$$

The total mass loss is $(m_1 - m_2)/m_1$, hence

$$C = \ln(1 - \text{TML})/\left(\exp(-E_a/RT)2t^{1/2}\right) \tag{3}$$

In order to determine the reaction constant, it is necessary to know the activation energy. Another test, ASTM E1559, can be used to obtain this value. Activation energy can also be obtained from quartz crystal microbalance (QCM) data by performing a thermogravimetric analysis (TGA). In the absence of either of these data sets, we can estimate the activation energy by considering the molecular residence time.

B. Residence Time

Desorbed or outgassed molecules will travel in straight lines (ignoring electrostatic, drag, and gravitational effects) until impacting another surface. There, the molecule temporary adheres to the surface and establishes thermal equilibrium. The molecule remains attached until, due to random events, it acquires enough energy to escape the electronic attraction to the surface. The time spent on the surface is known as residence time and is given by

$$\tau_r = \tau_0 \exp\left(E_a/RT\right) \tag{4}$$

where τ_0 is the oscillation period of the molecules on the surface, with typical value $\sim 10^{-13}$ seconds.[8] Once the molecule acquires sufficient energy to escape, it will leave with direction following the cosine law from the surface normal.[10] In this sense, molecules act in a fashion similar to photons; in fact, thermal radiation transport codes are commonly used by contamination community to compute deposition rates.

For most species, the residence time will be very short except on surfaces below that gas material's condensation temperature. Figure 2 plots equation 4 over a range of temperatures for three activation energies: 3.5, 9, and 12 kcal/mol. These three curves correspond to three species modeled in the results section. They are supposed to correspond to nitrogen, water, and an arbitrary hydrocarbon. Please note that these activation energies are not meant to be the physical values. For instance, the activation energy of water is actually closer to 11 kcal/mol. The activation energies were selected such that the gases demonstrated the expected behavior: nitrogen only condensed on a cryo pump, water condensed on an LN2 cooled plate, but not on a room temperature surface, and the hydrocarbon condensed even at room temperature. From the Arden-Buck equation, the saturation vapor pressure of water at 2×10^{-5} Torr is approximately 160K (-112°C). Water is thus expected to condense on the 100K surface, and in fact we see that $\tau_r > 10^6$s given our simulation activation energy. On the 300K surface, τ_r is only 3.6×10^{-7}, indicating that this surface is too warm for condensation to take place.

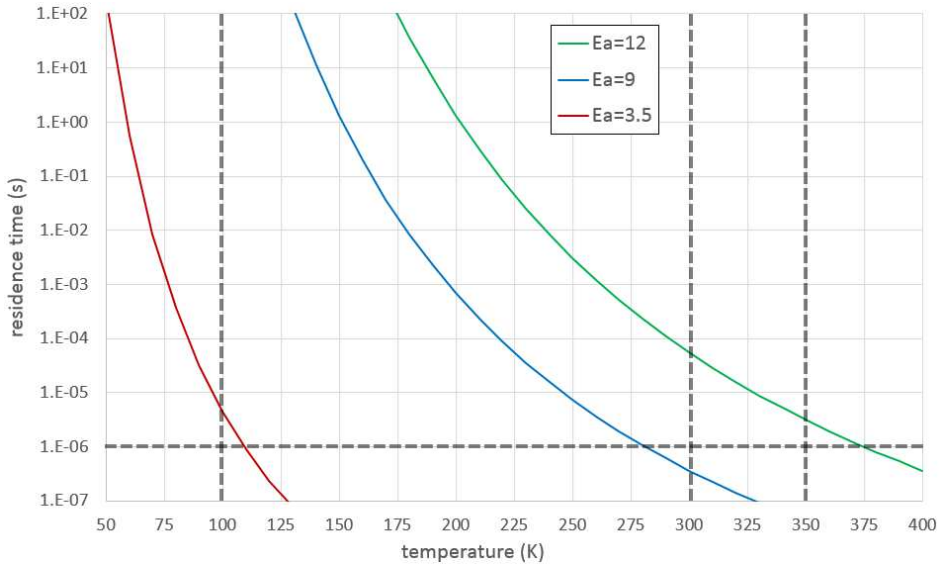

Figure 2. Variation of residence time with activation energy (kcal/mol). Note that although these values were used subsequently to model nitrogen, water, and a hydrocarbon, the values are not supposed to correspond to the actual physical activation energies. E_a for water is actually closer to 11 kcal/mol.

C. Desorption

A contaminant layer will build up as long as the arrival rate exceeds the rate of departure. For a deposition thickness less than a monolayer, the rate of molecules leaving the surface is given by first order desorption,[10]

$$\frac{dN}{dt} = \frac{1}{\tau_r} N \tag{5}$$

D. Numerical Implementation

The model is implemented in a particle tracing code described in more detail in the following section. The implementation consists of two parts: particle impact handler, and an outgassing source. Upon impacting a surface, the code computes residence time using equation 4 at the temperature of the impacted surface element. If $\tau_r \leq \Delta t$, the particle is re-emitted. The particle is first pushed to the surface by replacing its position with the impact location, $\mathbf{x}_p = \mathbf{x}_1 + t\,(\mathbf{x}_2 - \mathbf{x}_1)$, where t is the parametric position from a line-plane intersection algorithm. Velocity magnitude, v_S is then sampled from the Maxwellian speed distribution function f_M at the surface temperature. The particle's new speed is set from $v' = |\mathbf{v}| + \alpha_S(v_S - |\mathbf{v}|)$, where α_a is the surface thermal accommodation coefficient. In our simulations, full accommodations $\alpha_a = 1$ was assumed. The new velocity direction follows the Lambertian law, with the following algorithm used to sample from the cosine distribution:

$$\begin{aligned}
\sin\theta &= R_1 \\
\cos\theta &= \sqrt{1 - \sin^2\theta} \\
\psi &= 2\pi R_2 \\
\hat{\mathbf{v}}_L &= \hat{\mathbf{v}}_{t1}\sin\theta\cos\psi + \hat{\mathbf{v}}_{t2}\sin\theta\sin\psi + \hat{\mathbf{v}}_n\cos\theta
\end{aligned}$$

The new particle velocity is then $\mathbf{v}' = v'\hat{\mathbf{v}}_L$.

On the other hand, if $\tau_r > \Delta t$, the particle is adsorbed into the surface layer. Numerically, this involves removing the particle and incrementing surface count of material i (corresponding to the particle) by the specific weight, $\Delta N_i = w_{sp}$. The counts can be related to surface layer thickness by $h = N(4/3)\pi r^3/A_{el}$, where r is the molecular radius. Outgassing is implemented as a source called by the main loop at every time step. The algorithm computes the amount of outgassed mass for each component from equation 1. The mass, converted to number of molecules, is added to the surface layer count for that particular species. The

incremental value for each surface element j is scaled by the local area ratio, $dN_j = (dm_{outgas}/m)A_j/A_{tot}$, where A_{tot} is the total surface area of the component. Next, the code loops through all surface elements, and for each computes the amount of mass lost to desorption per equation 5. For cold surfaces, this value will be too small to produce particles at the used macroparticle weight. But if a finite number of particles is generated, the code depletes the surface layer accordingly. The overall algorithm can be summarized by the pseudocode below:

```
load material data (density, molecular radius, TML, ...)
load component data (temperature, total mass, cleanliness level, ...)
initialize surface data structures

for each timestep:
   #particle push
   for each particle:
      if surface impact:
         compute residence time
                 if greater than time step:
                    deposit to surface layer
                 else:
                    re-emit following cosine law

   #outgassing model
   for each component:
      compute mass outgassing mass loss
      add to surface layer

   #desorption
   for each surface element:
      compute desorption loss
      inject particles with cosine distribution
      deplete surface layer
```

III. Transport Code

The surface model was implemented in Contamination Transport Simulation Program (CTSP), a 3D C++ code for modeling molecular and particulate contamination developed by Particle In Cell Consulting LLC (PIC-C). Instead of tracing a ray from start to finish before moving to another, as is done in Monte-Carlo based radiative heat transfer / view factor codes, CTSP pushes many simulation particles concurrently. In this respect CTSP resembles the Direct Simulation Monte Carlo (DSMC) or Particle In Cell (PIC) methods. However, the CTSP push does not utilize a volume mesh. Such a mesh is used in PIC to compute self-induced forces, and in DSMC to group particles for collisions. Since CTSP focuses on free-molecular neutral flow applications, eliminating the volume mesh helps reduce the memory footprint. The volume mesh can however be used for diagnostics, as demonstrated later in the Results sections. Particle data is scattered to the grid similar to the PIC technique to compute density. In cases where external forces need to be considered (such as for electrostatic return of ionized molecules, or trajectory calculation of dust particles in an airflow), properties at the particle position are interpolated from point-cloud data using inverse distance weighing,

$$\mathbf{f}(x) = \begin{cases} \dfrac{\sum_i^N w_i(\mathbf{x})\mathbf{f}_i}{\sum_i^N w_i(\mathbf{x})} & d(\mathbf{x},\mathbf{x_i}) \neq 0 \\ \mathbf{f}_i & d(\mathbf{x},\mathbf{x_i}) = 0 \end{cases} \tag{6}$$

where the kernel $w_i(\mathbf{x})$ is $d(\mathbf{x},\mathbf{x}_i)^{-p}$.

The geometry bounding the simulation is represented by a triangular and/or quadrilateral surface mesh generated by COTS CAD programs. The geometry used in our modeling study is shown in Figure 3. This

setup describes an arbitrary vacuum chamber. The chamber contains an internal thermal shroud, two inlet ports, two cryogenic pumps, and a scavenger plate. The chamber also contains three support platens, with the central one supporting a test article containing a smaller "electronics box" assumed to be hotter than the main body. The traced particle is injected at one of the ports, and after undergoing many surface collisions, finds itself trapped in the narrow region between the shroud and the chamber wall. Given longer time, the particle would eventually impact one of the two cryopumps or the scavenger plate, and be adsorbed.

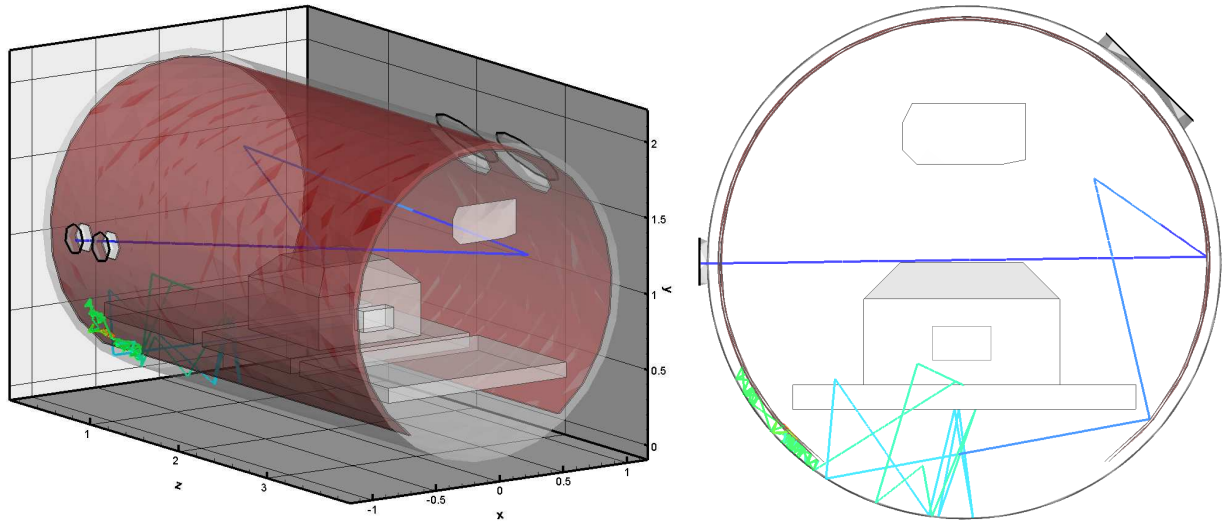

(a) Side view (b) Front view

Figure 3. Plot of a single particle trace and also the setup geometry. The particle is injected at a port plate, and after a large number of surface impacts, ends up in the narrow space between the thermal shroud and the chamber wall. The cryopumps, small scavenger plate, platens, and test hardware can also be seen.

Particles are injected into the simulation either from the surface model described in the previous section, or from gas flow sources. So far, only a Maxwellian flow source has been implemented. This source injects a prescribed volumetric flow rate Q (m^3/s) at a given temperature and drift velocity. The source can inject composite gas consisting of multiple species. This allows us to easily model air leaks, where the injection would consist of nitrogen, oxygen, argon, helium, and other trace gases. The source works by sampling a random direction vector from the isotropic distribution[11] and multiplying it by a magnitude sampled from the Maxwellian speed distribution function using the method of Birdsall.[12] A drift component is then added. Particle position is integrated from $\mathbf{x}^{k+1} = \mathbf{x}^k + \mathbf{v}^{k+0.5}\Delta t$. However, unless external forces are applied, $\mathbf{v}^{k+0.5} = \mathbf{v}^k$, and the Leapfrog algorithm reduces to the Euler forward method.

The code uses octree for efficient lookup of surface elements to consider during surface hit checks (another octree is used to store the point-cloud data, if any). Octree is a data structure in which the 3D domain is subdivided into 8 equal-sized octants. Surface elements wholly or partially located in an octant are added to a storage dataset in that octant. If the number of elements exceeds some predefine threshold (10 in our case), the octant is subdivided into eight new pieces. Figure 4 visualizes the components of the octree four levels down from the top. All surface elements possibly blocking a particle during a push from $\mathbf{x_1}$ to $\mathbf{x_2}$ can then be retrieved using the following simple un-optimized recursive pseudocode:

```
Node.getElements(element_list, x1, x2):
        if (!containsBox(x1,x2)) return

        if (leaf_node):
                add all unique elements to element_list
        else:
                for (i=1:8): child[i].getElements(element_list, x1, x2)
```

The code then iterates through the list of returned surface triangles. For each, it computes the line-plane

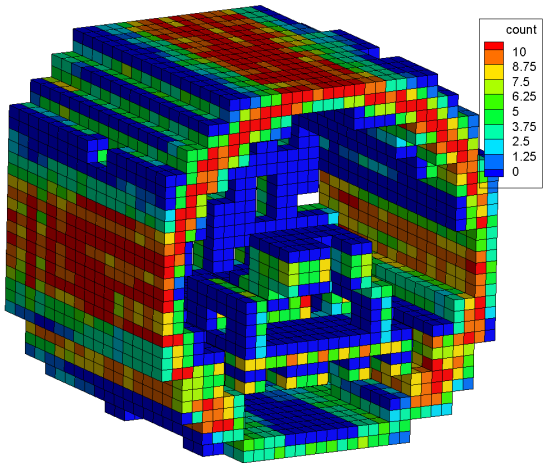

Figure 4. Level four octree elements with a non-zero surface element count.

intersection parametric location,

$$t = \frac{\mathbf{n} \cdot (\mathbf{x}_1 - \mathbf{x}_0)}{\mathbf{n} \cdot (\mathbf{x}_1 - \mathbf{x}_2)} \tag{7}$$

where $\mathbf{n}$ and $\mathbf{x}_0$ are the surface element normal and centroid, respectively. Element with intersection in the valid range $t \in (0, 1]$ are sorted in ascending order, and checked for point in triangle/quad.

CTSP uses a JSON-like syntax to specify program flow in the input file. Example input is shown below:

```
#load surface
surface_load_stl{file_name:"chamber.stl"}

#define volume mesh, before materials are loaded
volume_mesh{dx:0.05, dy:0.05, dz:0.05}

#materials
solid_mat{name:black_paint, mass: 100}
solid_mat{name:pump, mass:100}

gas_mat{name:water, mass: 18, spwt: 5e13, Ea:9, C:10}
gas_mat{name:hc1, mass: 94, spwt: 1e10, Ea:12, C:10}
gas_mat{name:n2, mass: 28, spwt: 1e14, Ea:3.5, C:3}

#define components
comp{name:ebox, mat:al, trapped_mass:1e-3, trapped_mat:[0.005*n2, 0.05*water, 0.75*hc1],
        surf_h:1e-10, surf_mat:water, temp:350}
comp{name:shroud, mat:black_paint, temp:100}

#enable outgassing
source_outgassing{}

#surface source
source_maxwellian{comp:port1, Q:1e-9, mats:[0.75*n2, 0.25*o2], temp:300, v_drift:100}

#attach probes
probe{comp:port1, type:qcm}

#specify output
surface_save_vtk{skip:10000, file_name:"surf"}
volume_save_vtk{skip:10000, file_name:"field", vars:[pressure,nd-ave.n2,nd-ave.water]}
```

```
#run simulation
ctsp{dt:1e-6, nt:60000, diag_start:1, diag_skip:20}
```

IV. Results

A. Gas Injection

The model is next demonstrated with several cases covering various events typical of vacuum chamber operations and EP testing. The first example is a simple gas injection into a vacuum chamber. This situation could mimic a post-test chamber repress. But in the realm of EP testing, it could also represent experimental pressure increase in facility effects studies. Nitrogen gas was injected at one of the chamber ports, by associating a Maxwellian source with the port component. The chamber was initially assumed to be completely empty, hence this solution describes the partial pressure of the injected gas. Figure 5 shows four gas density contours, taken 20,000 time steps apart. In this and all subsequent simulations, the time step $\Delta t = 10^{-6}$s. The thermal component and spacing between the port and the cutout in the thermal shroud results in some injected gas molecules impacting the back side of the shroud and scattering into the gap between the shroud and the chamber wall. This behavior demonstrates itself as a ring of higher density along the perimeter of the chamber. We also observe increased gas density around the test article. The top part of the article has a line of sight to the source, so it receives direct flux in addition to reflected flux from the walls. Re-emission from the test article further increases the gas density.

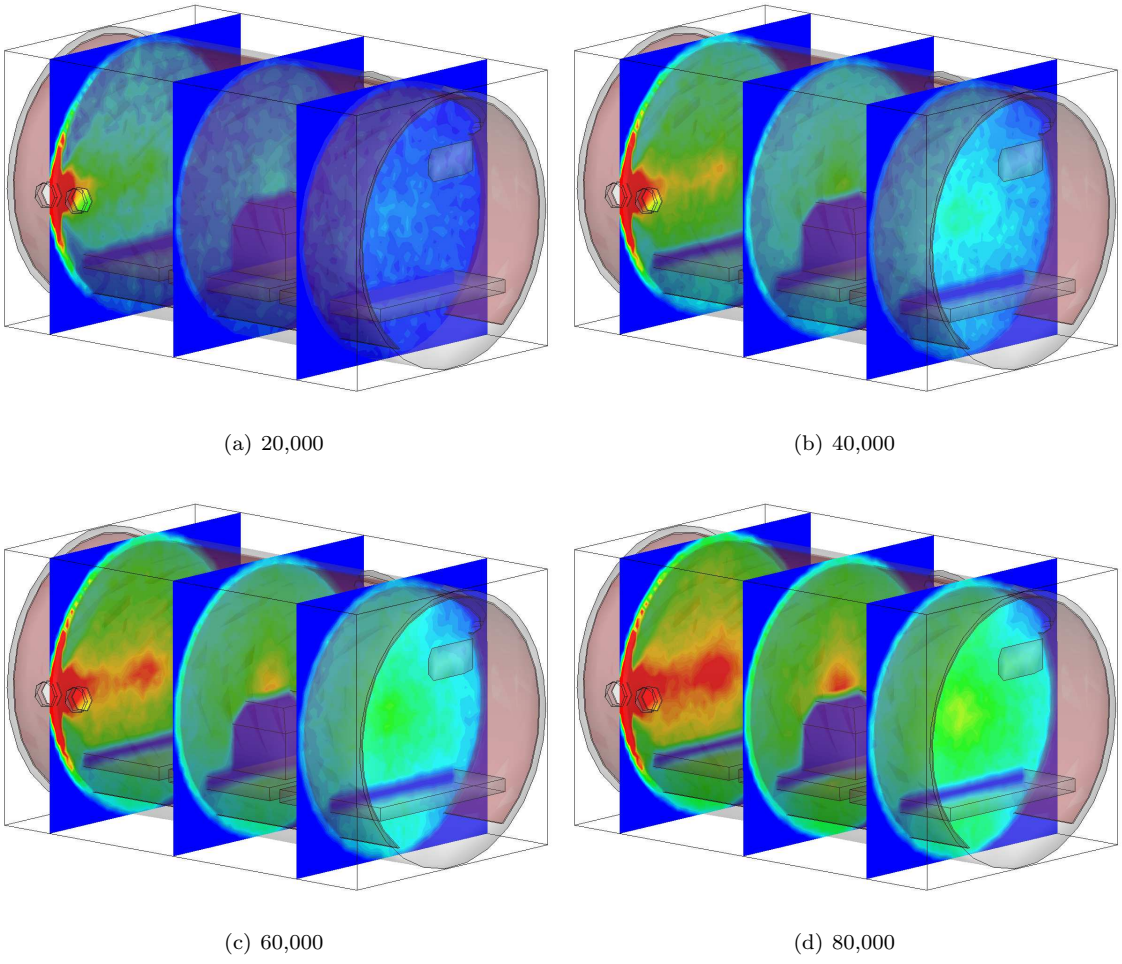

(a) 20,000 (b) 40,000

(c) 60,000 (d) 80,000

Figure 5. Gas pressure after a different number of time steps. Some of the injected gas can be seen to become trapped behind the thermal shroud.

B. Outgassing

Next, outgassing is demonstrated. This case used the same geometry as above, but there was no gas injection from the port. Instead, the electronics box was assumed to contain a trapped hydrocarbon. Figure 6 shows a time evolution of the hydrocarbon density. The platens, thermal shroud, and the chamber wall were assumed to be at 300K. The scavenger plate temperature was set to 100K, while the cryopump temperatures were 12K. Because this simulated hydrocarbon has a non-negligible residence time at 300K, it condenses on impact with any surface. This demonstrates itself as the increased surface layer thickness on all surfaces with a direct line of sight to the box. The highest deposition is seen on the downstream platen, as well as on the back face of chamber. The deposition is however not limited to the surfaces with direct line of sight. According to our model, $\tau_r = 5.25 \times 10^{-5}$s at 300K, and hence small fraction of the deposited material will outgass from the shroud, platens, and other 300K surfaces. This re-emission then contributes to deposition outside the direct line of sight from the ebox. In radiative heat transfer, this would correspond to gray body re-emission, or a sticking coefficient $0 < \alpha_{sc} < 1$. The residence time on the 100K scavenger plate is 168×10^{13}s, which is effectively an infinitely long time. The scavenger (and correspondingly the vacuum pump) would have $\alpha_{sc} = 0$.

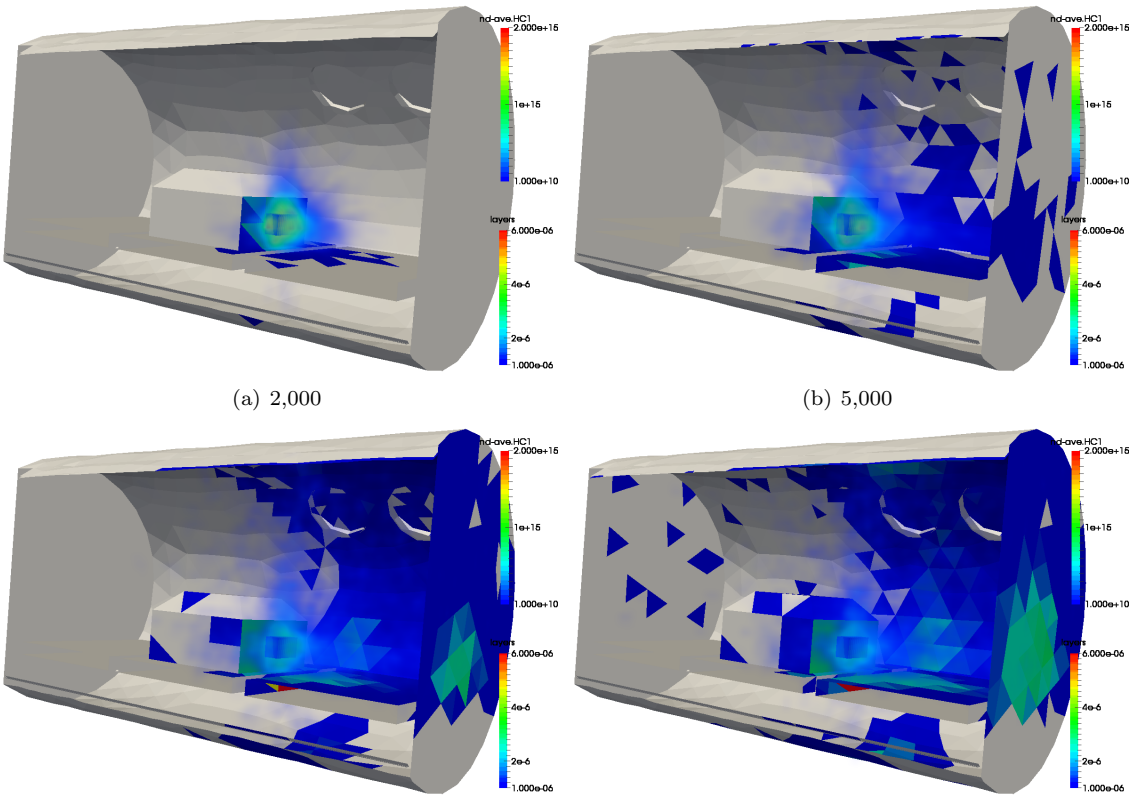

(a) 2,000 (b) 5,000

(c) 20,000 (d) 40,000

Figure 6. Time evolution of a hydrocarbon outgassing from the electronics box,

C. Combined Model

Next, the model was extended by including additional trapped gases, as indicated in Table 1. The activation energies followed the model presented previously in Figure 2. The test article and the e-box were also coated with 1Å thick surface layer of water. Additionally, the thermal shroud temperature was lowered to 100K. The simulation was run for 100,000 time steps, and the number of simulation macroparticles versus time step is shown in Figure 7. The specific weights for water and nitrogen were identical. A lower weight ($5 \times 10^4 w_{hc} = w_{water}$) was used for the hydrocarbon, due to the difference in densities. We can see that the chamber pressure is initially dominated by water molecules, but eventually water is depleted, and nitrogen takes over as the dominant species. This is indeed the behavior seen during vacuum testing as reported by

RGA probes. This figure also captures the initial flash off of water from the surface layer. It is seen as a spike in the count of water molecules. Subsequently, water population starts exhibiting exponential decay characteristic of the diffusion process.

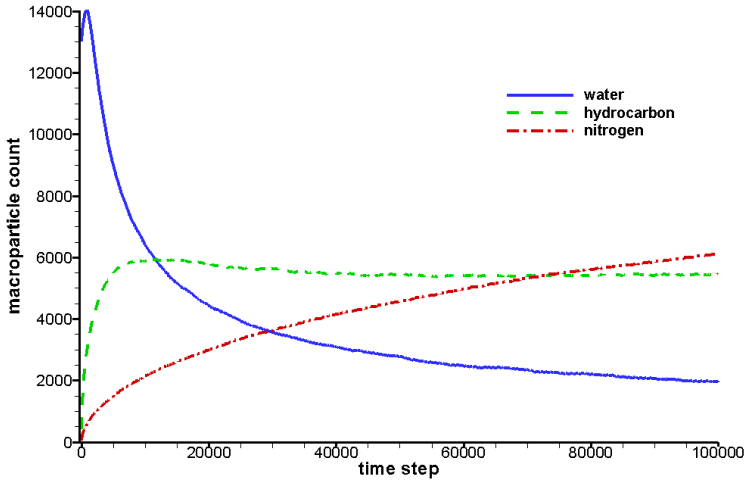

Figure 7. Macroparticle counts. Specific weights for nitrogen and water were identical and 50,000× larger than hydrocarbon weight.

	Nitrogen	Water	Hydrocarbon
Test Article (300K)	0.025	0.25	0
Electronics Box (350K)	0.005	0.050	0.75

Table 1. Mass composition in grams of the trapped gases for the "combined model" simulation.

Figures 8 and 9 illustrate the individual species densities after 40,000 time steps. In these simulations, the thermal shroud temperature was reduced to 100K. This configuration thus corresponds to a cold cycle in a thermal vacuum test campaign. At this temperature, water is expected to condense ($\tau_r = 4.67 \times 10^6$), while nitrogen is not ($\tau_r = 4.46 \times 10^{-6}$s). This is indeed the result we obtain. Nitrogen gas density demonstrates higher levels of uniformity than water due to reemission from the shroud. For both gases we see reduced concentration below the platens. This is also the expected behavior. If the simulation was run for a significantly longer time to deplete the trapped nitrogen outgasing from the test article, we would see the nitrogen density eventually equalize. Due to time constraints it is not practical to wait for days for all trapped materials to outgas prior to commencing EP testing. During the early phases, we can thus expect elevated pressures near the test equipment, especially if it is composed of porous or organic materials, or has not seen extensive vacuum time in the past. Including the contributions from the three species, the total pressure for this particular setup varies over two orders of magnitude. While far away from the test object the pressure is about 10^{-6} Torr, near the high temperature electronics box, it exceeds 10^{-4} Torr. The latter pressure is sufficient to form a discharge in high voltage components. Yet, if the pressure is measured only by a single pressure gauge located in the chamber wall, the test conductor may not be aware of the localized high pressures, and risk damaging a sensitive component. For this reason, the Magnetospheric Multiscale (MMS) mission thermal vacuum campaign utilized 15 ion gauges located in a close vicinity to the spacecraft to monitor local pressure prior to high voltage turn on.[13]

Figure 9 shows the same data but from a different angle. The slice was selected to pass through one of the cryopumps. We notice that the simulation does not predict any noticeable pressure drop near the pumps. This is a direct consequence of the free molecular model. Since the molecular collisions are infrequent, individual gas molecules do not influence each other, and there is no mechanism for the gas to communicate the adsorption at the pump. In collisional flow, density decrease in one region would result in increased diffusive flux. Here, the molecules are not aware of the presence of the pump until they strike it. The pump thus does not actually "pump" the gas, it simply acts as a sink for molecules that happen to impact it. For this reason, it is imperative that the pump has a good line of sight to the chamber. Long ducts or baffling

can significantly reduce the pumping speed.

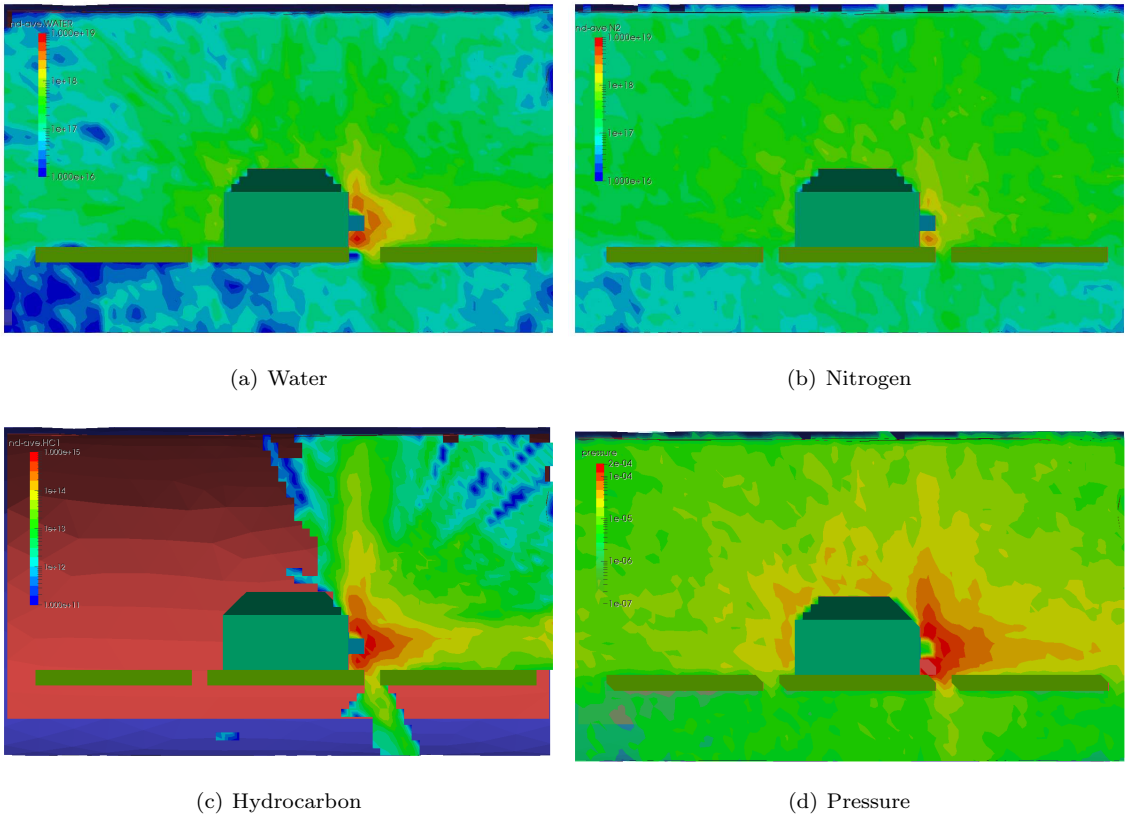

(a) Water (b) Nitrogen

(c) Hydrocarbon (d) Pressure

Figure 8. Species densities and total pressure after 40,000 time steps, side view.

Figure 10 is an attempt to visualize the contributions to the total pressure. In this plot, water is shown in blue, while nitrogen is shown in red. Near the test object, the pressure is dominated by the water vapor, while further away, nitrogen dominates. This is again the expected behavior.

D. Thermal Shroud Impact

We can also investigate the impact of the thermal shroud temperature on the pressure. From our three simulated species, only water is sensitive to the shroud temperature over the considered temperature range: nitrogen is expected to never condense, while the shroud would need to be raised to bake out temperatures to prevent condensation of the hydrocarbon. Figure 11 shows time evolution of water vapor concentration. In each sequence, the plot on left corresponds to a warm 300K shroud. The shroud in the right sets is at 100K. Besides noticing larger partial pressures with a warm shroud, we can also notice increased deposition on the cryopumps and the scavenger plate. This result demonstrates mass conservation, since in a closed system

$$\Gamma_{hw} A_{hw} = \Gamma_{sink} A_{sink} \tag{8}$$

where Γ_{hw} and A_{hw} are the molecular flux and area of the outgassing hardware, and "sink" corresponds to all surfaces cold enough to collect the outgassed matter. With a cold shroud, $A_{sink} = A_{shroud} + A_{scav} + A_{pump}$, but at 300K, the sink area reduces to $A_{sink} = A_{pump}$. The deposition on the cryopumps is thus expected to increase according to $1 + A_{shroud}/(A_{pump} + A_{scav})$. Since $A_{shroud} \gg (A_{pump} + A_{scav})$, the pump flux is greatly increased.

E. Electric Propulsion Testing

The final example illustrates application of the surface model towards electric propulsion testing. In this example, the test geometry was modified from the previous cases. The thermal shroud was removed, as were

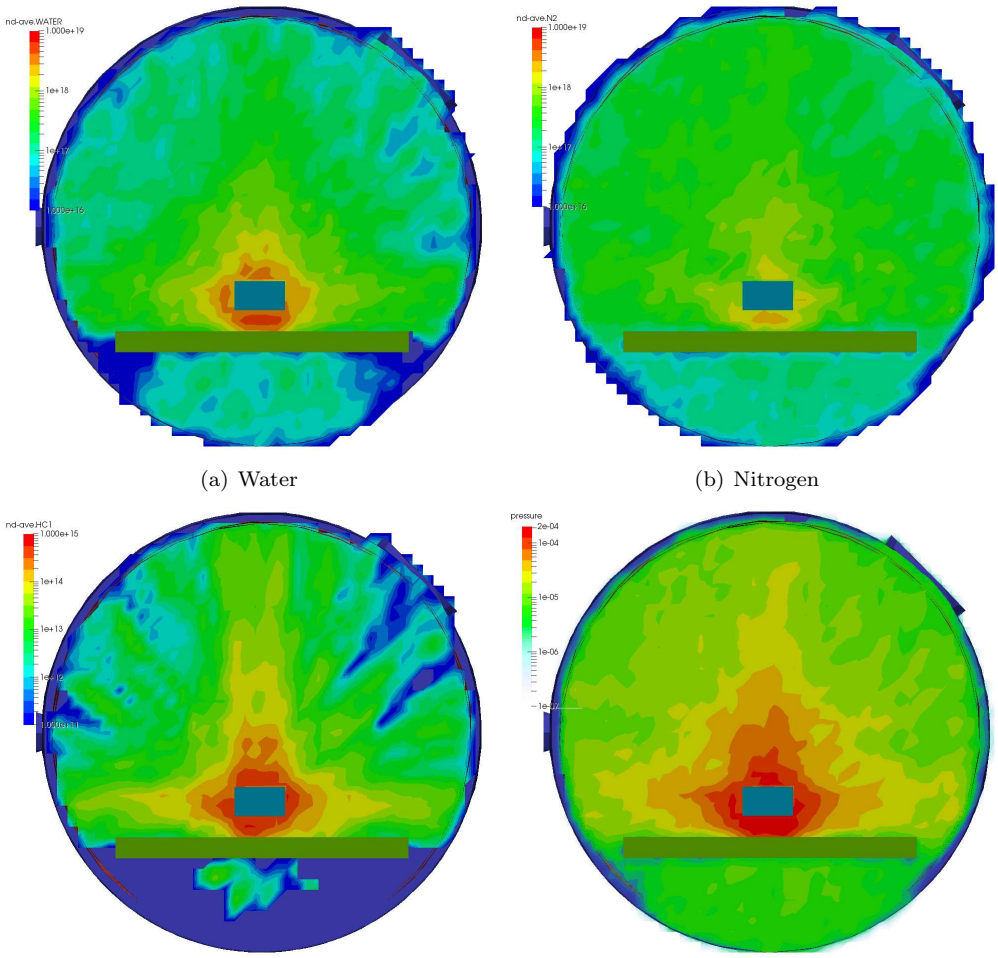

(a) Water (b) Nitrogen

(c) Hydrocarbon (d) Pressure

Figure 9. Species densities and combined pressure after 40,000 time steps, end view. The thermal shroud reduced set to 100K.

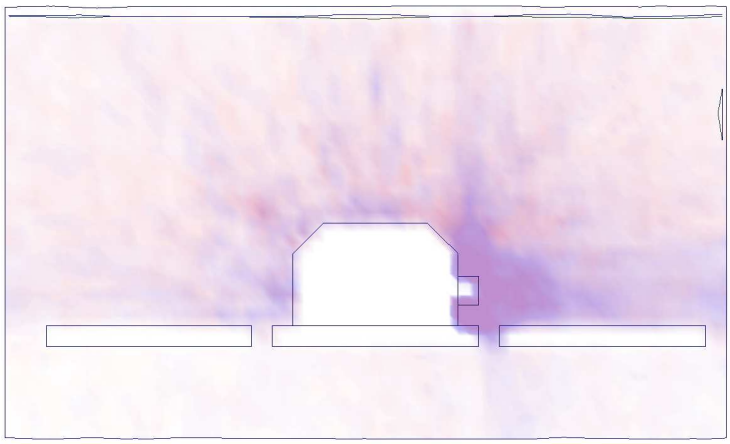

Figure 10. Combined pressure. Water is plotted in blue, while nitrogen is shown in red.

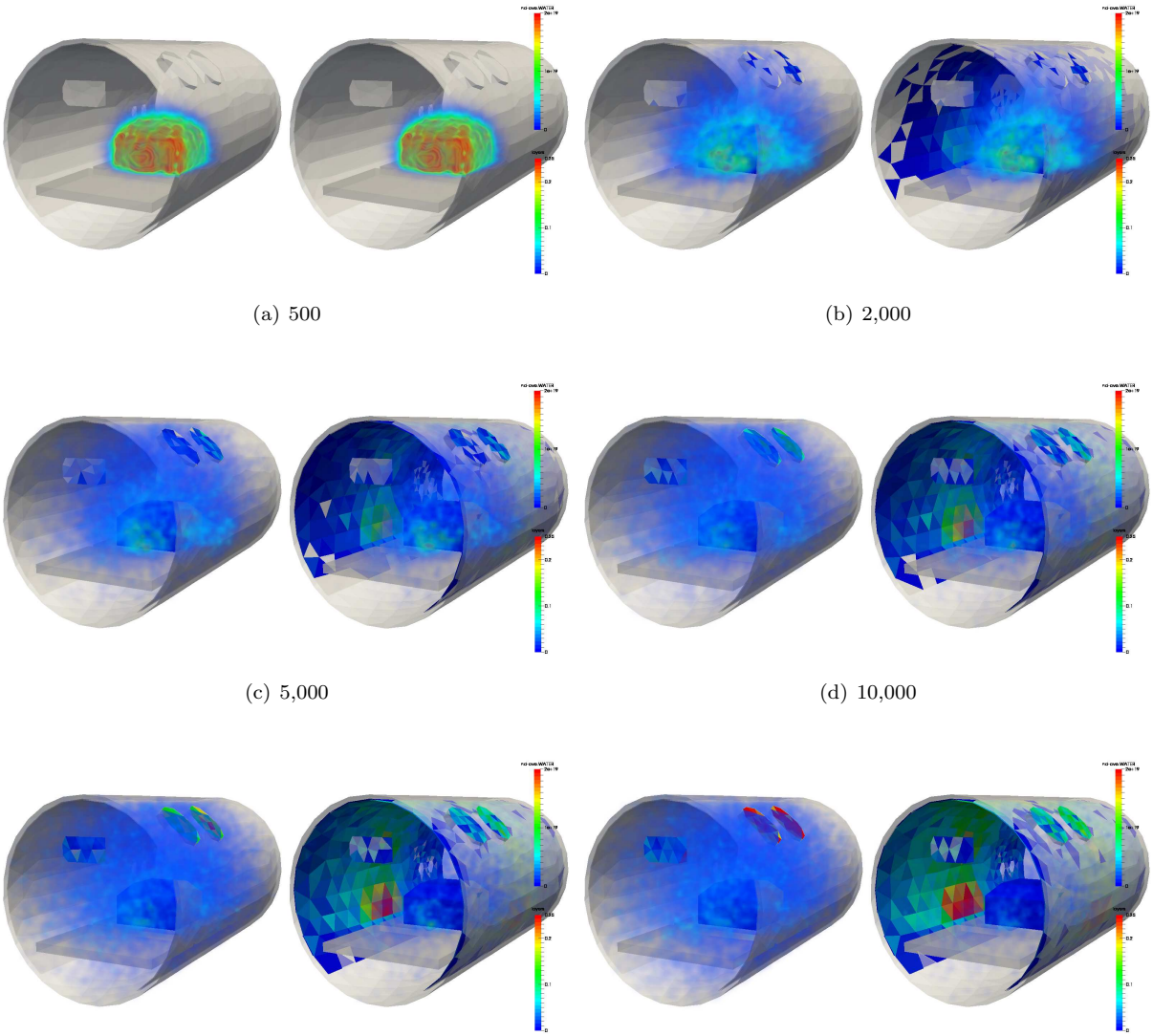

(a) 500 (b) 2,000

(c) 5,000 (d) 10,000

(e) 20,000 (f) 40,000

Figure 11. Comparison of thermal shroud temperature impact on water concentration at different timesteps. The case on left corresponds to a warm plateau with the shroud set to 300K, while the case on right is a cold setpoint with a 100K shroud. We can see increased deposition on the cryopumps with the warm shroud, since the total collection area is significantly reduced.

the platens and the test hardware. Instead, a Hall thruster and a support beam structure were introduced. The scavenger plate was also expanded in size to act as a beam dump. In this setup, xenon ions and neutrals were injected at the annular exit plane of the thruster. The flow rates were such that $Q_{Xe^+} = 10Q_{Xe}$. Drift velocities were 17km/s and 50m/s for the ions and neutrals, and source temperatures were 50,000K and 1000K, respectively. The high ion source temperature was simply used to obtain beam divergence. Since CTSP does not contain a plasma solver, the ions were treated as free molecular gas without any forces acting on them.

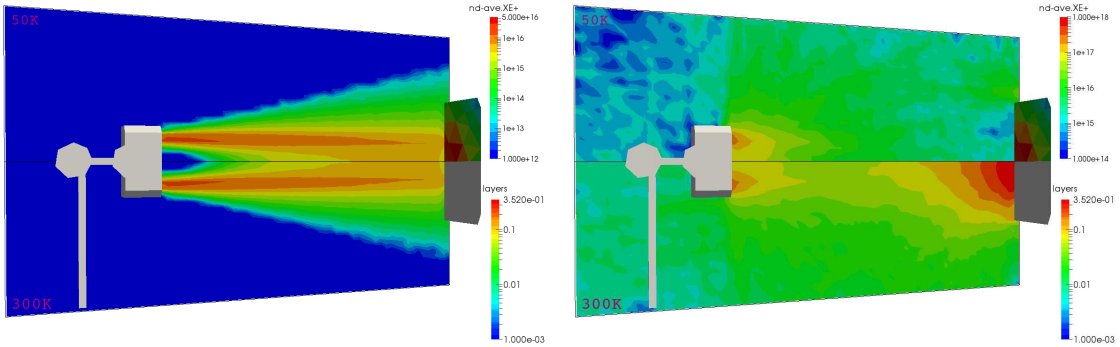

(a) Ions (b) Neutrals

Figure 12. Ion and neutral density for cold (top) and warm (bottom) beam dump.

Figure 12 compares the ion and neutral densities for a cold (top) and warm (bottom) beam dumps. The beam dump temperature has no impact on the ion density, since ions are neutralized at the point of impact. Conversion of ions into neutrals at the surface can be seen in the neutral plot, Figure 12(b). With the cold dump, we see a gradual decrease in neutral density as we move away from the thruster along the centerline. The neutral density increases just above the cold plate, since the chamber wall is not cold enough to condense the ion beam. Surface contours also indicate the presence of deposition. We notice xenon partial pressure behind the thruster to be about 2 orders of magnitude smaller than in the plume. This backflow is due to reflection of the primary beam off the backwall and also to scattering from the chamber wall of the un-ionized propellant. With a warm target, the propellant gas no longer condenses, and is instead reemitted following the cosine distribution. As such, we see xenon pressure in front of the beam dump increases. The pressure behind the thruster is now of similar magnitude as the average pressure in front of the thruster. In this work we did not consider sputtering, which would act as an additional contributor to chamber pressure.

The plots in Figure 13 show snapshots from a dynamic simulation. The beam dump was initially set to 50K, which was cold enough to condense xenon. The ions undergo surface neutralization, and contribute to the xenon atom surface layer thickness. In Figure 13(b) we can see the thickness of the deposited material on the beam dump increasing. Next, xenon injection was initiated at one of the ports, in a manner similar to Section A. We note that the gs injection results in an overall increase in gas concentration, but bulk of increase is in the region behind the thruster (near the port). If the chamber pressure was measured here, an incorrect conclusion could be reached about the background pressure in the thruster near plume. Then, between time steps 30,000 and 40,000, the beam dump temperature is increased at a linear rate. This temperature increase results in an impressive flash-off of the collected propellant in Figure 13(e). It should be noted that this flash-off was driven solely by the changing surface temperature - illustrating the benefit of the surface model presented in this paper for capturing dynamic system response. The flashed off xenon gas continues expanding towards the opposite side of the chamber until filling the chamber in 13(h).

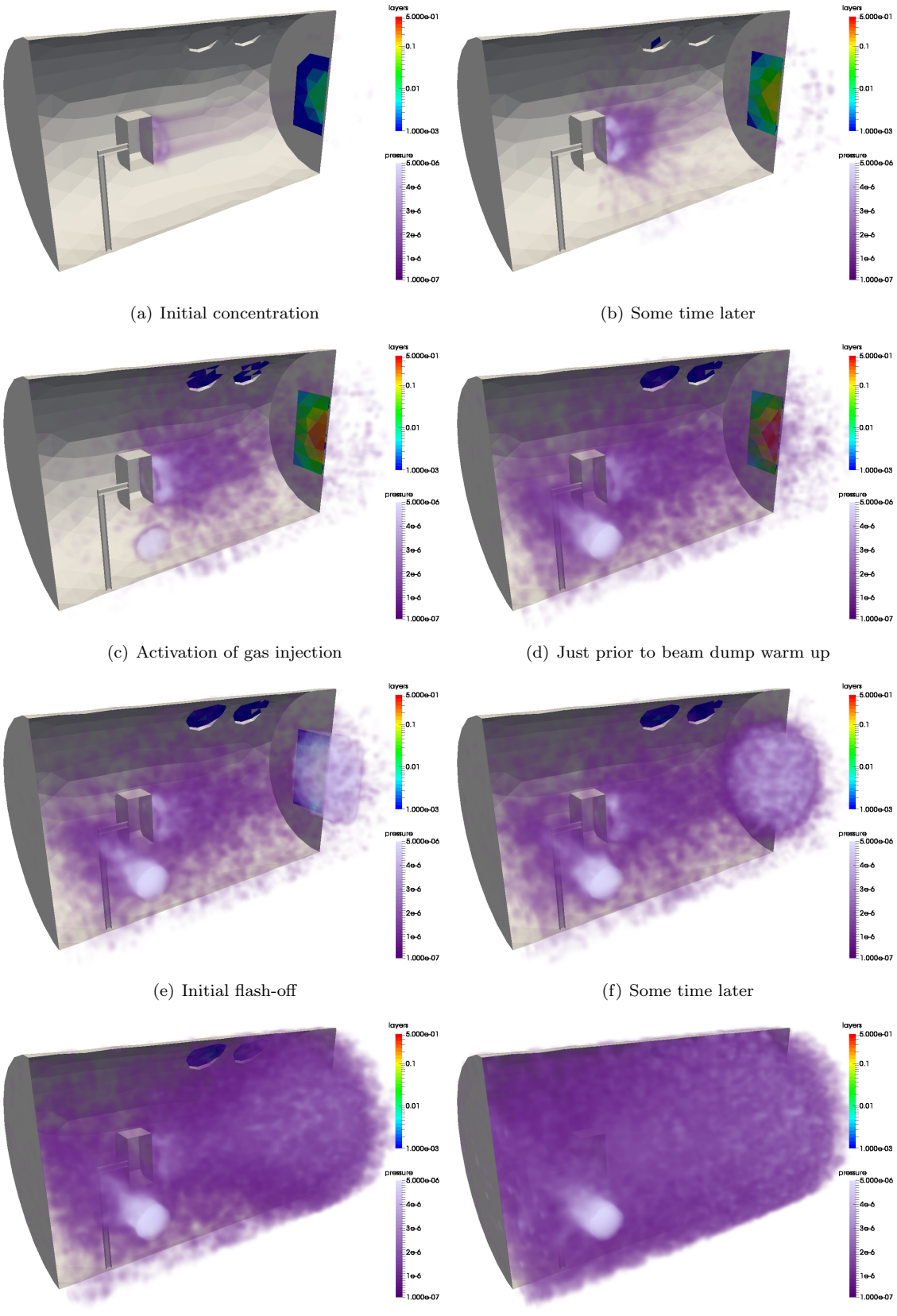

(a) Initial concentration

(b) Some time later

(c) Activation of gas injection

(d) Just prior to beam dump warm up

(e) Initial flash-off

(f) Some time later

(g) Expansion of flashed-off gas

(h) Final concentration

Figure 13. Neutral density for an EP application. The beam dump is initially cold enough to condense the propellant gas. Later, gas injection at one of the ports begins. Next, the beam dump temperature is increased, resulting in a flash off of the collected propelant.

V. Conclusion and Future Work

In this paper, we presented a new model for capturing surface interactions in vacuum and electric propulsion applications. Instead of utilizing a sticking coefficient to determine whether an impacting molecule should be reflected, the model computes the residence time using the surface temperature and the activation energy of the molecule material. If the residence time is greater than the simulation time step, the molecule is adsorbed into a surface layer. In addition, the model supports modeling outgassing, which is a slow release of gases trapped in the native material by diffusion. The model allows us to capture physics beyond what is possible with state of the art EP modeling tools. This includes desorption of surface water, outgassing of materials in the vacuum chamber, and rapid flash off of condensed matter as surfaces are warmed up. These features were demonstrated by implementing the algorithm in a 3D free molecular flow simulation code, CTSP.

Although the results presented here are promising, additional work remains to develop a truly realistic model for the space-surface interface. Such a model will need to include sputtering, charging, current emission from secondary electrons and other sources, particulate deposition, as well as synergistic effects. Development of these features is ongoing and will be presented in the future.

References

[1]Walker, M., Gallimore, A., Cai, C., and Boyd, I., "Pressure Map of a Facility as a Function of Flow Rate to Study Facility Effects," *38th AIAA Joint Propulsion Conference*, Indianapolis, IN, 2002.

[2]Boyd, I., VanGilder, D., and Liu, X., "Monte Carlo Simulation of Neutral Xenon Flows of Electric Propulsion Devices," *25th International Electric Propulsion Conference*, Cleveland, OH, 1997.

[3]Randolph, T., Kim, V., Kaufman, H., Kozubsky, K., Zhurin, V., and Day, M., "Facility Effects on Stationary Plasma Thruster Testing," *23th International Electric Propulsion Conference*, Seattle, WA, 1993.

[4]Walker, M., *Effects of facility backpressure on the performance and plume of a Hall thruster*, Ph.D. thesis, University of Michigan, Ann Arbo, MI, 2005.

[5]Hofer, R., Peterson, P., and Gallimore, A., "Characterizing Vacuum Facility Backpressure Effects on the Performance of a Hall Thruster," *27th International Electric Propulsion Conference*, Pasadena, CA, 2001.

[6]Gibbons, M., Kirtley, D., VanGilder, D., and Fife, J., "Flexible Three-Dimensional Modeling of Electric Thrusters in Vacuum Chambers," *39th AIAA Joint Propulsion Conference*, Huntsville, Al, 2003, AIAA-2003-4872.

[7]Brieda, L., *Development of the Draco ES-PIC Code and Fully-Kinetic Simulation of Ion Beam Neutralization*, Master's thesis, Virginia Tech, 2005.

[8]Tribble, A., *Fundamentals of Contamination Control*, SPIE, 2000.

[9]Campbell, W. A. and Scialdone, J. J., "Outgassing data for selecting spacecraft materials," *NASA Technical Report 1124,revision 3. Goddard Space Flight Center.*, 1993.

[10]O'Hanlon, J. F., *User's Guide to Vacuum Technology*, Wiley & Sons, 2003.

[11]Particle In Cell, "Loading Isotropic Velocity Distribution Function," `https://www.particleincell.com/2012/isotropic-velocity/`, 2012.

[12]Birdsall, C. and Langdon, A., *Plasma physics via computer simulation*, Institute of Physics Publishing, 2000.

[13]Rosecrans, G., Brieda, L., and Errigo, T., "MMS Observatory TV Results Contamination Summary," *28th Space Simulation Conference*, Baltimore, MD, 2014.